Anti-Tumoral Effects of A Benzimidazolyl Carbamate Ester Derivative on Head and Neck Squamous Carcinoma Cell Lines

Alice Nicolai
Sapienza University of Rome: Universita degli Studi di Roma La Sapienza
Valentina Noemi Madia
Sapienza University of Rome: Universita degli Studi di Roma La Sapienza
Antonella Messore
Sapienza University of Rome: Universita degli Studi di Roma La Sapienza
Alessandro De Leo
Sapienza University of Rome: Universita degli Studi di Roma La Sapienza
Davide Ialongo
Sapienza University of Rome: Universita degli Studi di Roma La Sapienza
Valeria Tudino
Sapienza University of Rome: Universita degli Studi di Roma La Sapienza
Elisabetta Tortorella
Sapienza University of Rome: Universita degli Studi di Roma La Sapienza
Luigi Scipione
Sapienza University of Rome: Universita degli Studi di Roma La Sapienza
Samanta Taurone
Sapienza University of Rome: Universita degli Studi di Roma La Sapienza
Tiziano Pergolizzi
Sapienza University of Rome: Universita degli Studi di Roma La Sapienza
Marco Artico
Sapienza University of Rome: Universita degli Studi di Roma La Sapienza
Roberto Di Santo
Sapienza University of Rome: Universita degli Studi di Roma La Sapienza
Roberta Costi
Sapienza University of Rome: Universita degli Studi di Roma La Sapienza
Susanna Scarpa (susanna.scarpa@uniroma1.it)
Universita degli Studi di Roma La Sapienza Dipartimento di Medicina Sperimentale
https://orcid.org/0000-0002-3169-3968

Research Article

Keywords: benzimidazole, head and neck squamous cell carcinoma, apoptosis, epithelial-mesenchymal transition, tubulin

Posted Date: February 16th, 2021

DOI: https://doi.org/10.21203/rs.3.rs-233855/v1

Abstract

Nocodazole is a well-known anti-proliferative agent, thanks to its anti-microtubule activity. Herein we report a benzimidazolyl carbamate ester derivative, namely RDS 60, as structural analog of this compound. We evaluated the anti-neoplastic properties of RDS 60 in two human head and neck squamous cell carcinoma (HNSCC) cell lines. We found that RDS 60 significantly inhibited replication of both HNSCC without inducing any significant cytotoxic effect on non-transformed human dermal fibroblasts. The treatment of the two cell lines with 1 μM RDS 60 for 24 hours determined the incapacity of cells to develop normal bipolar mitotic spindles contemporaneously to a block of the cell cycle in G2/M and to cytoplasmic accumulation of cyclin B1. Moreover, doubling the dosage of RDS 60, an activation of apoptosis in both HNSCC was observed. Additionally, RDS 60 treatment reversed the epithelial-mesenchymal transition and inhibited cell migration and extracellular matrix infiltration of both HNSCC. These results demonstrate that this compound has a potent effect in blocking cell cycle, inducing apoptosis and inhibiting cell motility and invasion of the two HNSCC cell lines. Therefore, the ability of RDS 60 to attenuate the malignant phenotype of HNSCC suggests its potential role as an interesting and powerful tool for new approaches in treating these tumors.

Introduction

Nocodazole is a benzimidazol-2-yl carbamate ester derivative that interacts with microtubules by targeting tubulin. In fact, nocodazole exerts a high affinity for beta tubulin, developing hydrogen bonds between the single beta subunits and consequently inhibiting first the aggregation of alpha and beta subunits and then the interaction among tubulin heterodimers; this altered state finally induces the depolymerization of microtubules [1, 2]. The impairment of microtubules polymerization determines an alteration of mitotic spindle organization with the consequent incapacity to carry out mitosis [3, 4]. Whenever cells with high replication rate are treated with nocodazole, they are not able to organize a normal bipolar mitotic spindle, so that they do not complete mitosis and are blocked in G2 or M phase of cell cycle. Yet, the prolonged arrest in pro-metaphases is a starting point for apoptosis [5]. Despite its antitumoral activity, nocodazole did not reach the clinical phase so far [6]. On the other hand, several previous reports have suggested that benzimidazole is the most prominent heterocycle having good cytotoxic properties against different types of cancer cell lines [7-9]. Therefore, we decided to deepen our knowledge on the anti-tumor activity of a benzimidazole derivative structurally related with nocodazole that we previously synthesized and reported [10], namely RDS 60 (Fig. 1). To this aim, we evaluated the activity of RDS 60 in terms of anti-mitotic and apoptosis inducer agent and we tested its potential anti-tumoral efficiency directed to human head and neck squamous cell carcinomas (HNSCC), a group of tumors detectable in various regions of the oral cavity, oropharynx, hypopharynx and larynx. We chose these types of neoplasms because they are extremely aggressive; in fact, almost 50% of the newly diagnosed HNSCC has a survival rate below 5 years [11]. HNSCC are collocated at the sixth position among malign tumors more diffuse in the world [12] and they are all characterized by a poor prognosis, mainly due to metastases, to the development of multiple primary tumors and to local and regional often

inoperable relapses [13, 14]. The presence of distant metastases at the moment of diagnosis is associated to the high mortality rate of HNSCC [15] since the chemotherapy used for metastatic disease gives often low responses [16, 17].

Herein, we demonstrated that our benzimidazol-2-yl carbamate ester RDS 60 was capable to impair tubulin assembling in the mitotic spindle, to block the cell cycle in G2 phase, to induce apoptosis and to reverse the invasive phenotype of two HNSCC cell lines.

Materials And Methods

RDS 60 synthesis

RDS 60 (ethyl (5-((1H-pyrrol-1-yl)methyl)-1H-benzo[d]imidazol-2-yl)carbamate) (Fig. 1a) was synthesized as previously described [10]. However, we modified the first two reaction steps in order to improve the overall reaction yields. Indeed, we applied a reduction reaction according to Moore et al. [18] of the commercially available carboxylic acid into alcohol that was subsequently converted in the corresponding benzyl chloride (Fig. 1b) via an aliphatic nucleophilic substitution. The subsequent synthetic steps resemble the ones previously reported [10]. Therefore, we report the details of the first two synthetic steps since the other ones can be found in ref. 10. Melting point (°C), recrystallization solvent, yield (%), chromatographic system, IR, ^{1}H NMR, formula, Mr and analyzed elements for derivative RDS 60 agreed with the ones previously described [10]. RDS 60 samples used for biological evaluation were 99% pure as determined by elemental analysis.

Synthesis of 1

A solution of $AlCl_3$ (3.77 g; 28.28 mmol) in THF dry (4.6 mL) was added dropwise into a solution of 3,4-dinitrobenzoic acid (5 g; 23.57 mM) and $NaBH_4$ (3.21 g; 84.85 mmol) in THF dry (46 mL) at 0 °C within 20 min. The reaction was stirred at 25 °C for 1 hour (h) and for 2 h to reflux and then poured into ice-cold water (115 mL). The pH was adjusted to 7 with 1 N HCl and the mixture was extracted with ethyl acetate (3 x 50 mL). The collected extracts were washed with brine (3 x 100 mL) and dried. Removal of the solvent furnished crude residue that was washed with ethyl acetate in order to discard the boron salt, yielding intermediate 1 (3.37 g, 72.1 %) as a yellow solid.

Synthesis of 2

To a solution of compound 1 (16.27 g, 81.85 mM) in $CHCl_3$ (126 mL) was added PCl_5 (6.63 g, 31.85 mM) portionwise at 0 °C within 15 min. The reaction mixture was stirred at 0 °C for 15 min and at 25 °C for 2.5 h and then poured into ice-cold water. The organic layer was washed with 5% w/v Na_2CO_3 (3 x 100 mL) and with $NaCl_{ss}$ (3 x 100 mL) and dried. Removal of the solvent furnished the crude compound 2 that underwent to the following step without further purification.

Cell cultures and treatment

Two HNSCC cell lines were utilized: tongue carcinoma CAL27 and pharynx carcinoma FaDu (ATCC, USA), and one human dermal fibroblast primary culture HF [19, 20]. Cells were grown in RPMI 1640 medium with 10% fetal calf serum (FCS), 2 mM glutamine and 50 U/mL penicillin-streptomycin (Sigma-Aldrich). The compound RDS 60 was solubilized in dimethylsulfoxide (DMSO) (Sigma) for a 10 mM stock solution and utilized to final concentrations from 100 nM to 10 µM for 24 and 48 h. Control cells were treated with equivalent amounts of DMSO in every experiment.

Cytotoxicity assay

To determine cytotoxicity, a sulforhodamine-B colorimetric assay was performed: $5x10^3$ cells were plated in 96-well plates, grown for 24 h and then treated with 100 nM, 1, 2.5, 5, 10 µM RDS 60 for 24 and 48 h. Cells were then fixed with 50% trichloroacetic acid for 1 h to 4 °C and stained for 30 min to room temperature (RT) with 0.4% sulforhodamine-B in 1% acetic acid. Excess dye was removed by washing four times with 1% acetic acid. Protein-bound dye was dissolved in 10 mM Tris pH 10 and optical density was determined at 510 nm using a microplate reader.

Flow cytometry analysis

Cells were seeded in 60-mm plates, grown for 24 h and then treated with 1 µM RDS 60 or equivalent amounts of DMSO for 24 h. The cells were harvested by trypsinization, washed twice with cold PBS, fixed in 70% ethanol at 4°C overnight. Cells were rinsed twice with PBS and incubated with 50 µL of RNAse (100 µg/mL, Sigma) to ensure that only DNA was stained, and 200 µL of Propidium Iodide (PI) (50 µg/mL, Sigma). Cell cycle analysis was performed using a FACS CantoII equipped with 488nm laser and DIVA Software (BD Biosciences). The cells were first gated using a forward vs. side scatter (FSC vs. SSC) strategy, and upon 488 nm laser excitation, PI fluorescence was then detected above 580 nm. Data were analyzed using Flow Jo software (Flow Jo LLC, OR, USA).

Immunofluorescence

Cells were grown on Labteck chamber slides (Nunc) for 24 h and then treated with 1µM RDS 60 or with DMSO for 24 h. Cells were washed with PBS with Ca/Mg (washing buffer) and fixed with 4% buffered paraformaldehyde (Sigma Aldrich) for 20 min at 4 °C, then permeabilized with PBS, 5% FCS, 0.5% TritonX100 for 30 min at RT and incubated for 1 h to RT with the primary monoclonal antibody to beta-tubulin (1:100 diluted; Immunological Sciences). Alternatively, cells were permeabilized with 0.1 % TritonX100 for 10 min to RT, incubated with 3% BSA for 1 h to RT and incubated with the primary rabbit polyclonal antibody to cyclin B1 in 0.1% BSA (1:200 diluted; Elabscience, USA) overnight at 4°C. Cells were washed twice with washing buffer and incubated with the secondary anti-mouse or anti-rabbit antibody FITC conjugated (1:400 diluted; Molecular Probes) for 1 h to RT. Cells were washed twice with washing buffer and DNA was stained with Hoechst for 15 min to RT. The slide was mounted with ProLong-Antifade (Life Technologies) and analyzed by a fluorescence microscope (Olympus BX52). Image acquisition and processing were conducted by IAS 2000 software.

Western blot analysis

Cells were seeded in 100-mm plates, grown for 24 h and treated with 2.5 μM RDS 60 or with equivalent amounts of DMSO for 24 h. Cells were then scraped in lysis buffer (1% Triton, 0.1% sodium dodecyl sulfate, 150 mM NaCl, 50 mM Tris HCl pH 7.4, 2 mM EDTA) with protease inhibitor cocktail (Roche Applied Science, Germany) for 30 min at 4 °C. Lysates were centrifuged at 16,000xg for 15 min at 4 °C and the supernatant was collected. Protein concentration was evaluated using Protein Concentration Assay (Bio-Rad Laboratories, CA, USA). Protein lysates (50-100 μg) were separated by molecular weight with 10, 12 or 14% SDS-PAGE and then transferred onto nitrocellulose membranes. Membranes were blocked for 1 h to RT in 5% nonfat dry milk and incubated with primary antibodies opportunely diluted in PBS-Tween overnight at 4°C, washed in Tris-buffered saline with 0.1% Tween-20 and incubated with horseradish-peroxidase-conjugated-anti-mouse/rabbit-IgG (1:5000; Sigma-Aldrich, MO, USA) for 1 h to RT. Filters were then developed using enhanced chemiluminescence (Super Signal West Pico Chemiluminescence Substrate; Thermo Fisher Scientific, USA) using Kodak X-Omat films (Kodak, USA). Primary antibodies were: mouse anti-poly (ADP-ribose)-polymerase (PARP-1) (diluted 1:500; Santa Cruz Biotechnology, TX, USA); mouse anti-cleaved-caspase 8 (diluted 1:500; Cell Signaling Technology, MA, USA); mouse anti-caspase 9 (diluted 1:500; Cell Signaling Technology); mouse anti-B-cell-lymphoma-2 (Bcl-2) (diluted 1:200; Santa Cruz Biotechnology); rabbit anti-Bcl-2-associated-X-protein (Bax) (diluted 1:250; Santa Cruz Biotechnology); rabbit anti E-cadherin (1:1000 diluted; GeneTex); rabbit anti N-cadherin (1:1000 diluted; GeneTex); rabbit anti-tubulin (diluted 1:4000; Immunological Sciences). Experiments were performed in triplicate, the bands from the blots were quantified using ImageJ v.1.48 software (National Institutes of Health, Bethesda, MD, USA), the mean values were calculated and expressed as densitometric units (DU).

Invasion assay

Invasion assay was performed with Matrigel Invasion Chambers (Corning) consisting of inserts with 8 μm pore membrane pretreated with Matrigel: $5x10^5$/mL cells were plated in serum-free medium plus DMSO or in serum-free medium plus 1 μM RDS 60 in the insert chamber, the lower chamber contained complete medium with FCS. After 18 h of culture the inserts were washed with PBS with Ca/Mg and fixed by 100% methanol for 20 min at 4 °C, washed twice with PBS with Ca/Mg and stained for 20 min at RT with haematoxylin. The inserts were then mounted on slides and the cells that migrated through the filter pores to the lower side of the membrane were counted by an optical microscope (Olympus BX52). Imagine acquisition and processing were conducted by IAS 2000 software.

Statistical analysis and graphic programs

All results were analyzed using one-way analysis of variance, and significance was evaluated using Tukey's honest significant difference post hoc test. All figures were created using Adobe Photoshop CS5 and all graphs were produced and statistical analyses conducted using Graph Pad Prism 5.0.

Results

Given the antitumoral activity of the benzimidazole-based small molecule nocodazole, we decided to deepen the activity of its analog belonging to our in-house library, namely RDS 60. Indeed, this compound shares the same benzimidazol-2-yl carbamate ester structure of nocodazole and differs for the replacement of the 2-thienyl substituent with its isostere1-pyrrolyl ring and for the reduction of the carbonyl group with a methylene one (Fig. 1).

To evaluate the effects of this new compound on cell viability and replication, two HNSCC cell lines were treated for 24 and 48 h with 100 nM, 1 μM, 2.5 μM, 5 μM, 10 μM RDS 60. A significant decrease in cell viability was evidenced at 24 h of RDS 60 treatment at 2.5 μM in CAL 27 and at 10 μM in FaDu; the decrease of proliferation became significant at 1 μM RDS 60 for both tumor cell lines at 48 h of treatment (Fig. 2). We repeated the time points of RDS 60 concentrations at 1, 10, 20, 30, 40 μM to calculate the EC_{50} that resulted 10.8 μM for CAL27 and 12.4 μM for FaDu at 24 h; 2.5 μM for CAL27 and 2.9 μM for FaDu at 48 h. To evaluate the cytotoxicity of the compound on normal somatic cells, human dermal fibroblasts HF were treated for 24 and 48 h with 100 nM, 1 μM, 2.5 μM and 10 μM RDS 60. This treatment led to decreased viability of HF only at the highest concentration of RDS 60 (Fig. 2). Therefore, we decided to perform the following experiments on tumor cells utilizing the compound at low concentrations around 1-2 μM, correspondent to not cytotoxic doses for HF.

Since the molecular target of nocodazole, analog of RDS 60, is tubulin, with the impairment of regular organization of microtubules, we analyzed whether RDS 60 could interfere in some way with tubulin and with its assembly into the mitotic spindle. To understand this aspect, we performed an immunofluorescent staining of beta-tubulin in both HNSCC untreated and treated with 100 nM and 1 μM RDS 60 for 24 h and then we observed the cells undergoing mitosis using a fluorescent microscope. We found that, while all untreated cells developed normal typical bipolar mitotic spindles, in the cells treated with both concentrations of RDS 60 it was impossible to find a normal mitotic spindle, because every mitotic spindle had abnormal shape and size, with tripolar or multipolar structure, certainly determining abortive mitosis (Fig. 2).

At this point we investigated whether RDS 60 could interfere with the cell cycle, so we analyzed both cell lines by flow cytometry at 24 h of treatment with 1 μM RDS 60 after staining with PI. We found that the treatment with 1 μM RDS 60 induced a notable increase of cells in G2/M phase and a parallel decrease of cells in S and G0/G1 phases. Specifically, RDS 60 increased the percentage of FaDu in G2/M from 27% to 69% and of CAL27 from 32% to 56% (Fig. 3). Consequent to this result, we evaluated cyclin B1 expression, since an increase of this protein is essential for the regular control of cell cycle transition from S to G2 and then to M phases [21]. So, we observed cyclin B1 by immunofluorescence and found that its staining was significantly enhanced upon 100 nM and 1 μM RDS 60 treatment for 24 h (Fig. 3). This result was in accordance with the increase of cells blocked in G2/M phase. Furthermore, we also showed that cyclin B1 localization was exclusively cytoplasmic in both treated and untreated cells and that the protein didn’t translocate into the nucleus (Fig. 3).

Since the block of cell cycle can represent a starting point for apoptosis, we investigated whether RDS 60 could induce apoptosis. Therefore, the expression of PARP-1 was evaluated, because its cleavage by caspase 3 occurs during the late phases of apoptosis so that cleaved PARP-1 is considered a marker of apoptosis. The two HNSCC were treated with 2 μM RDS 60 for 24 h and the decrease of uncleaved PARP-1 and the appearance of cleaved PARP-1 was observed in both (Fig. 4). In addition, other two protein correlated to apoptosis were evaluated: Bcl-2, an anti-apoptotic protein, and Bax, a pro-apoptotic Bcl-2-associated protein; because an increased Bax/Bcl-2 ratio is usually observed during apoptosis. We found that the pro-apoptotic protein Bax was up-regulated in both cell lines treated with 2 μM RDS 60 for 24 h, while the anti-apoptotic protein Bcl-2 was down-regulated exclusively in FaDu. The resulting Bax/Bcl2 ratio increased in both HNSCC upon treatment (Fig. 4), confirming the apoptotic response. Finally, the activation of initiator caspases 8 and 9 was analyzed, since the presence of proteolytic fragments of caspases is indicative of their activation and is an additional marker of apoptosis. Cleaved caspase 8 appeared in both cell lines after RDS 60 treatment, while caspase 9 was not modified by the treatment (Fig. 4), suggesting that RDS 60 activated apoptosis through the extrinsic pathway conducted by caspase 8.

We then investigated the epithelial-mesenchymal transition (EMT), that is a fundamental feature of malignant cells. Therefore, the modulation of two important markers of EMT, E-cadherin and N-cadherin, was analyzed and found that 24 h of 1 μM RDS 60 treatment was able to reverse EMT phenotype in both HNCSS. In fact, Western blot analysis showed that E-cadherin was low in basal conditions and increased after RDS 60 treatment, while N-cadherin from highly expressed in untreated cells became down-regulated after treatment (Fig. 5). In order to quantify the degree of malignity of these tumor cells, a Matrigel invasion assay was performed and both HNSCC basally showed a high rate of motility, while 16 h of 1 μM RDS 60 treatment was able to completely abolish this malignant attitude, since the number of cells able to migrate dramatically diminished when treated: from 71 to 17 for FaDu and from 92 to 23 for CAL27 (Fig. 5). The invasion capacity, represented by the number of cells capable to cross through the porous membrane, decreased significantly of 76 % in FaDu and 75 % in CAL27 after treatment (Fig. 5).

Taken together, these data demonstrated that RDS 60 played an important role not only in blocking the cell cycle and entering apoptosis, but also in reducing the invasive phenotype of HNSCC cells.

Discussion

During the last decades microtubules have constituted an interesting target in cancer therapy and the research still now is continuing to develop new targeted approaches to improve the existing compounds in order to increase their selectivity for tumor cells and decrease their unwanted side effects [22, 23]. Given our interest in developing new anti-cancer agents, we chose to design and synthesize a derivative of the microtubule targeting compound nocodazole and then to evaluate its anti-tumoral activity on two HNSCC cell lines. We demonstrated that this compound named RDS 60 was a potent inhibitor of proliferation in both tested HNSCC, while it did not exert any important cytotoxic effects on human dermal fibroblasts. The negative regulation performed by RDS 60 on cell replication was obtained by

targeting beta tubulin and hampering the assembly of bipolar mitotic spindles with the following abortion of mitosis, as we illustrated. In accordance with these events, RDS 60 arrested the cell cycle at the G2 phase, supported also by an impressive accumulation of cyclin B1 into the cytoplasm. It is known that cyclin B1 increases when the cell is approaching G2 phase and, before M phase, it is phosphorylated and must translocate from the cytoplasm into the nucleus in order to initiate mitosis [21]. We saw that cyclin B1 increased after RDS 60 treatment, but it remained totally localized into the cytoplasm; this information was first of all confirming that the cells were blocked in G2 phase and it was secondly suggesting that cyclin B1 was not activated and, for this reason, the cell cycle was interrupted between G2 and M phase. In a similar way, the microtubule depolymerizing drug nocodazole inhibits proliferation through a block of cell cycle in G2/M [24]. Usually, a cell undergoing a prolonged arrest in pro-metaphase starts towards apoptosis [5]; in fact, RDS 60, subsequently to its anti-proliferative effect, acted as an apoptosis inducer for both HNSCC, as demonstrated by the cleavage of PARP-1 and by the increase of the Bax/Bcl-2 ratio. This apoptosis followed the extrinsic pathway, as demonstrated by the specific cleavage for caspase 8 and not for caspase 9.

We then studied some features of HNSCC malignant and aggressive phenotype and found that both cell lines basally expressed low rates of E-cadherin and high rates of N-cadherin, confirming the typical EMT pattern of an invasive tumor [25]. We demonstrated that RDS 60 was able to reverse this EMT phenotype, by up-regulating E-cadherin and down-regulating N-cadherin in both HNSCC. The attitude to amplify cell motility and stroma infiltration reflects the clinical aggressive behavior usually represented by these tumors [26, 27] and, as expected, the two HNSCC showed a high basal rate of invasiveness into the extracellular matrix Matrigel. Interestingly, the treatment with RDS 60 markedly impaired this motility, reducing the invasion capacity up to 4 folds respect untreated cells. This ability to reduce the motility of HNSCC can be related to the target of RDS 60 represented by tubulin, which is the constituent not only of stable but also of dynamic microtubules; consequently, any kind of tubulin modification can reduce microtubules stability [28]. For example, it has been shown that post-translational deacetylation of tubulin alters the microtubule structure and promotes cell motility and the deacetylation of tubulin obtained with the overexpression of histone deacetylase 6 (HDAC6) is sufficient to enhance fibroblast motility [29]. We can hypothesize that RDS 60, through the destabilization of tubulin, can interfere with dynamic microtubules organization and consequently slow HNSCC cell mobility.

Taken together these data suggest that RDS 60 could represent a potential innovative anticancer agent for HNSCC, since this molecule is able to block tumor cells at G2 phase, to induce apoptosis and to direct the invasive cells toward a less malignant phenotype. Totally, we can present RDS 60 as a valuable additional tool capable to control and attenuate HNSCC malignity and aggressiveness.

Declarations

Compliance with Ethical Standards

Disclosure of potential conflicts of interest

The authors declare that there is no conflict of interest.

Research involving Human Participants and/or Animals

This research doesn't involve human participants and/or animals

Informed Consent

This research didn't use human participants or biological materials or any clinical data.

Ethics approval and consent to participate

This article does not contain any study with human participants or animals.

Availability of data and materials

All data and materials have been described and included in the manuscript.

Competing interests

All individual authors declare that they have no conflict of interest.

Funding

This research was supported by Sapienza University through the grant Ateneo "Sapienza".

Authors'contributions

Conception and design: Costi R, Di Salvo R, Artico M, S Scarpa

Development of chemical methodology: Messore A, De Leo A, Ialongo D, Tudino V, Scipione L

Development of biological methodology: Nicolai A, Tortorella E, Taurone S, Pergolizzi T

Writing: Scarpa S, Madia VN, Costi R

References

1. Florian S, Mitchison TJ (2016) Anti-microtubule drugs. Methods Mol Biol 1413:403-421.
2. Vasquez RJ, Howell B, Yvon AM, Wadsworth P, Cassimeris L (1997) Nanomolar concentrations of nocodazole alter microtubule dynamic instability in vivo and in vitro. Mol Biol Cell 8:973-985
3. Jordan MA, Thrower D, Wilson L (1992) Effects of vinblastine, podophyllotoxin and nocodazole on mitotic spindles. Implications for the role of microtubule dynamics in mitosis. J Cell Sci 102:401-416
4. Fraschini R (2017) Factors that Control Mitotic Spindle Dynamics. Adv Exp Med Biol 925:89-101.

5. Zhou J, Giannakakou P (2005) Targeting Microtubules for Cancer Chemotherapy. Curr Med Chem Anticancer Agents 5:65-71.
6. Wang Y, Zhang H, Gigant B, Yu Y, Wu Y, Chen X, Lai Q, Yang Z, Chen Q, Yang J (2016) Structure of a diverse set of colchicine binding site inhibitors in complex with tubulin provide a rationale for drug discovery FEBS J 283:102-111.
7. Shrivastava N, Naim MJ, Alam MJ, Nawaz F, Ahmed S, Alam O (2017) Benzimidazole Scaffold as Anticancer Agent: Synthetic Approaches and Structure-Activity Relationship. Arch Pharm 350 (6). https://doi.org/10.1002/ardp.201700040.
8. Madia VN, Messore A, Pescatori L, Saccoliti F, Tudino V, De Leo A, Bortolami M, Scipione L, Costi R, Rivara S, Scalvini L, Mor M, Ferrara FF, Pavoni E, Roscilli G, Cassinelli G, Milazzo FM, Battistuzzi G, Di Santo R, Giannini G (2018) Novel benzazole derivatives endowed with potent antiheparanase activity. J Med Chem 61:6918-6936.
9. Messore A, Madia VN, Pescatori L, Saccoliti F, Tudino V, De Leo A, Bortolami M, De Vita D, Scipione L, Pepi F, Costi R, Rivara S, Scalvini L, Mor M, Ferrara FF, Pavoni E, Roscilli G, Cassinelli G, Milazzo FM, Battistuzzi G, Di Santo R, Giannini G (2018) Novel symmetrical benzazolyl derivatives endowed with potent anti-heparanase activity. J Med Chem 61:10834-10859.
10. Massa S, Di Santo R, Artico M (1990) Potential antitumor agents. IV. Pyrrole analogues of oncodazole. J Heterocyclic Chemisty 27:1131-1133.
11. Yu AJ, Choi JS, Swanson MS, Kokot NC, Brown TN, Yan G, Sinha UK (2019) Association of Race/Ethnicity, Stage, and Survival in Oral Cavity Squamous Cell Carcinoma: A SEER Study. OTO Open 3 (4). https://doi.org/10.1177/2473974X19891126.
12. Gaździcka J, Golabek K, Strzelczyk JK, Ostrowska Z (2019) Epigenetic Modifications in Head and Neck Cancer. Biochem Genet 58:213-244. https://doi.org/10.1007/s10528-019-09941-1.
13. Zhang WL, Zhu ZL, Huang MC, Tang YJ, Tang YL, Liang XH (2019) Susceptibility of multiple primary cancers in patients with head and neck cancer: nature or nurture? Front Oncol 9:1275. https://doi.org/10.3389/fonc.2019.01275.
14. Tabor MP, Brakenhoff RH, Ruijter-Schippers HJ, van der Wal JE, Snow GB, Leemans CR, Braakhuis BJM (2002) Multiple head and neck tumors frequently originate from a single preneoplastic lesion. Am J Pathol 161:1051-1060.
15. Leemans CR, Braakhuis BJ, Brakenhoff RH (2011) The molecular biology of head and neck cancer. Nat Rev Canc 11:9-22.
16. Di Villeneuve L, Souza IL, Tolentino FDS, Ferrarotto R, Schvartsman G (2020) Salivary gland carcinoma: novel targets to overcome treatment resistance in advanced disease. Front Oncol https://doi.org/10.3389/fonc.2020.580141.
17. Ghafouri-Fard S, Gholipour M, Taheri M, Shirvani Farsani Z (2020) MicroRNA profile in the squamous cell carcinoma: prognostic and diagnostic roles. Heliyon 6(11). https://doi.org/10.1016/j.heliyon.2020.e05436.

18. Moore GF, Mambourger M, Gervaldo M, Poluektov OG, Rajh T, Gust D, Moore TA, Moore AL (2008) A bioinspired construct that mimics the proton coupled electron transfer between P680 and the Tyrz-His190 pair of photosystems II. J Am Chem Soc 130:10466-10467.
19. Taglieri L, Nardo T, Vicinanza R, Ross JM, Scarpa S, Coppotelli G (2017) Thyroid hormone regulates fibronectin expression through the activation of the hypoxia inducible factor 1. Bioch Bioph Res Comm 493:1304-1310.
20. Taglieri L, Saccoliti F, Nicolai A, Peruzzi G, Madia VN, Tudino V, Messore A, Di Santo R, Artico M, Taurone S, Salvati M, Costi R, Scarpa S (2020) Discovery of a pyrimidine compound endowed with antitumor activity. Invest New Drugs 38:39-49.
21. Hagting A, Jackman M, Simpson K, Pines J (1999) Translocation of cyclin B1 to the nucleus at phophase requires a phosphorylation-dependent nuclear import signal. Curr Biol 9:680-689.
22. Dumontet C, Jordan MA (2010) Microtubule-binding agents: a dynamic field of cancer therapeutics. Nat Rev Drug Discov 9:790-803.
23. Jordan MA, Wilson L (2004) Microtubules as a target for anticancer drugs. Nature Rev Cancer 4:253-265.
24. Kuhn M (1998) The microtubule depolymerizing drugs nocodazole and colchicine inhibit the uptake of Listeria monocytogenes by P388D1 macrophages. FEMS Microbiol Lett 160:87-90.
25. Liarte S, Bernabé-García A, Nicolás FJ (2020) Human skin keratinocytes on sustained TGF-β stimulation reveal partial EMT features and weaken growth arrest responses. Cells 9:306. https://doi.org/10.3390/cells9020306.
26. Yilmaz M, Christofori G (2009) EMT, the cytoskeleton, and cancer cell invasion. Cancer Metastasis Rev 28:15-33.
27. Boeve K, Melchers LJ, Schuuring E, Roodenburg JL, Halmos GB, van Dijk BA, van der Vegt B, Witjes MJ (2019) Addition of tumour infiltration depth and extranodal extension improves the prognostic value of the pathological TNM classification for early-stage oral squamous cell carcinoma. Histopathology 75:329-337.
28. Hubbert C, Guardiola A, Shao R, Kawaguchi Y, Ito A, Nixon A, Yoshida M, Wang XF, Yao TP (2002) HADAC6 is a microtubule-associated deacetylase. Nature 417:455-458.
29. Palazzo A, Ackerman B, Gundersen GG (2003) Tubulin acetylation and cell motility. Nature 421:230. https://doi.org/10.1038/421230a.

Figures

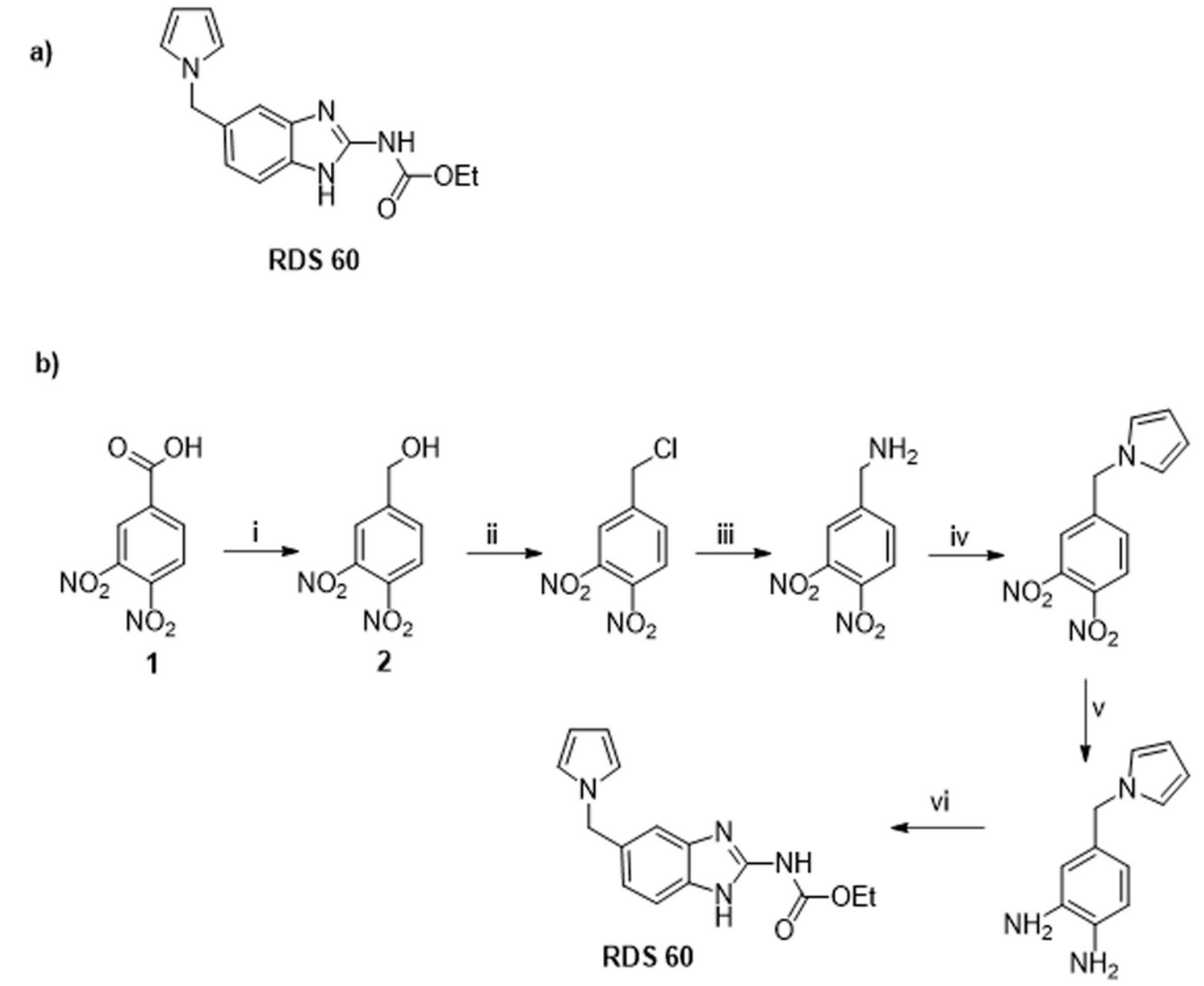

Figure 1

a) Chemical structure of RDS 60; b) Synthesis of RDS 60: i) AlCl3, NaBH4, THF dry, 0 °C to reflux, 3 h and 20 min; ii) PCl5, CHCl3, 0 °C to RT, 2 h and 45 min; iii) 1. (1s,3s)-1,3,5,7-tetraazaadamantane, NaI, EtOH abs., CHCl3, RT, 24 h, 2. HCl (37%), EtOH, 55 °C, 4 h, 3. Na2CO3(ss), RT; iv) 2,5-dimethoxytetrahydrofuran, AcOH, reflux, 5 min; v) H2/Pd, AcOEt, 45 °C, 4 h; vi) S-methylisothiourea, PTSA, EtOH, reflux, 45 min.

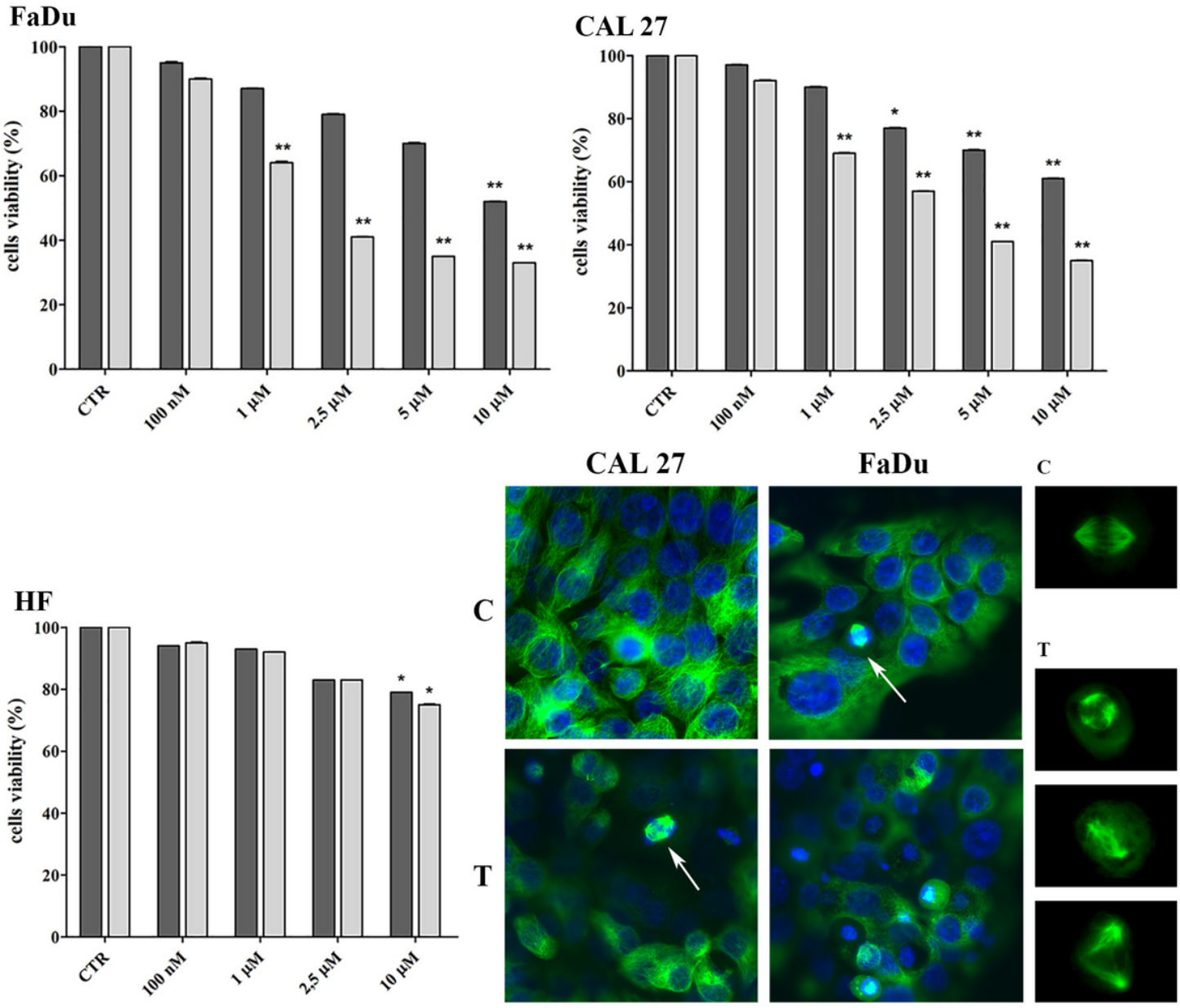

Figure 2

Cell viability of untreated (CTR) and RDS 60 treated FaDu, CAL27 and human normal fibroblasts (HF) expressed as percentages of alive cells ±SD. Treatments were performed for 24 h (dark gray) and 48 h (light gray). * p <0.01; ** p <0.001. Lower right panel - Immunofluorescence staining of beta tubulin on CAL27 and FaDu untreated (C) and treated with 1 µM RDS 60 (T) for 24 h. Magnification 40X. Smaller panels show mitotic spindles at higher magnification (100X) from untreated (C) and RDS 60 (T) treated cells.

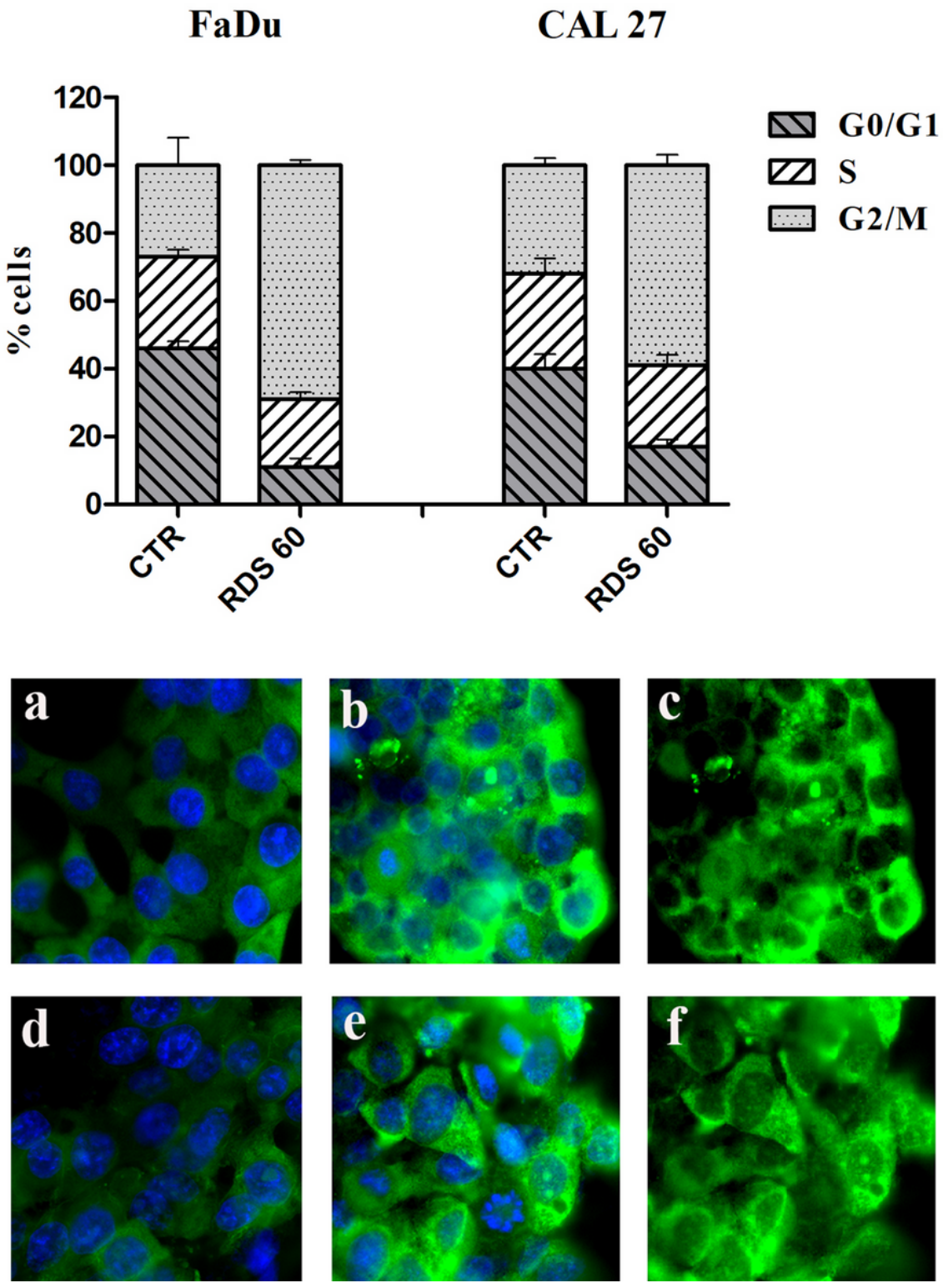

Figure 3

Upper panel - Cell cycle was investigated by flow cytometry analysis of DNA content after PI staining of FaDu and CAL27 cells untreated (CTR) and treated with 1 μM RDS 60 for 24 h. The histogram shows the media ±SD representative of results obtained from three independent experiments. Lower panel - Immunofluorescence staining of cyclin B1 on FaDu (a, b, c) and CAL27 (d, e, f) untreated (a, d) and

treated with 1 μM RDS 60 for 24 h shown with (b, e) and without (c, f) nuclear staining. Magnification 40X.

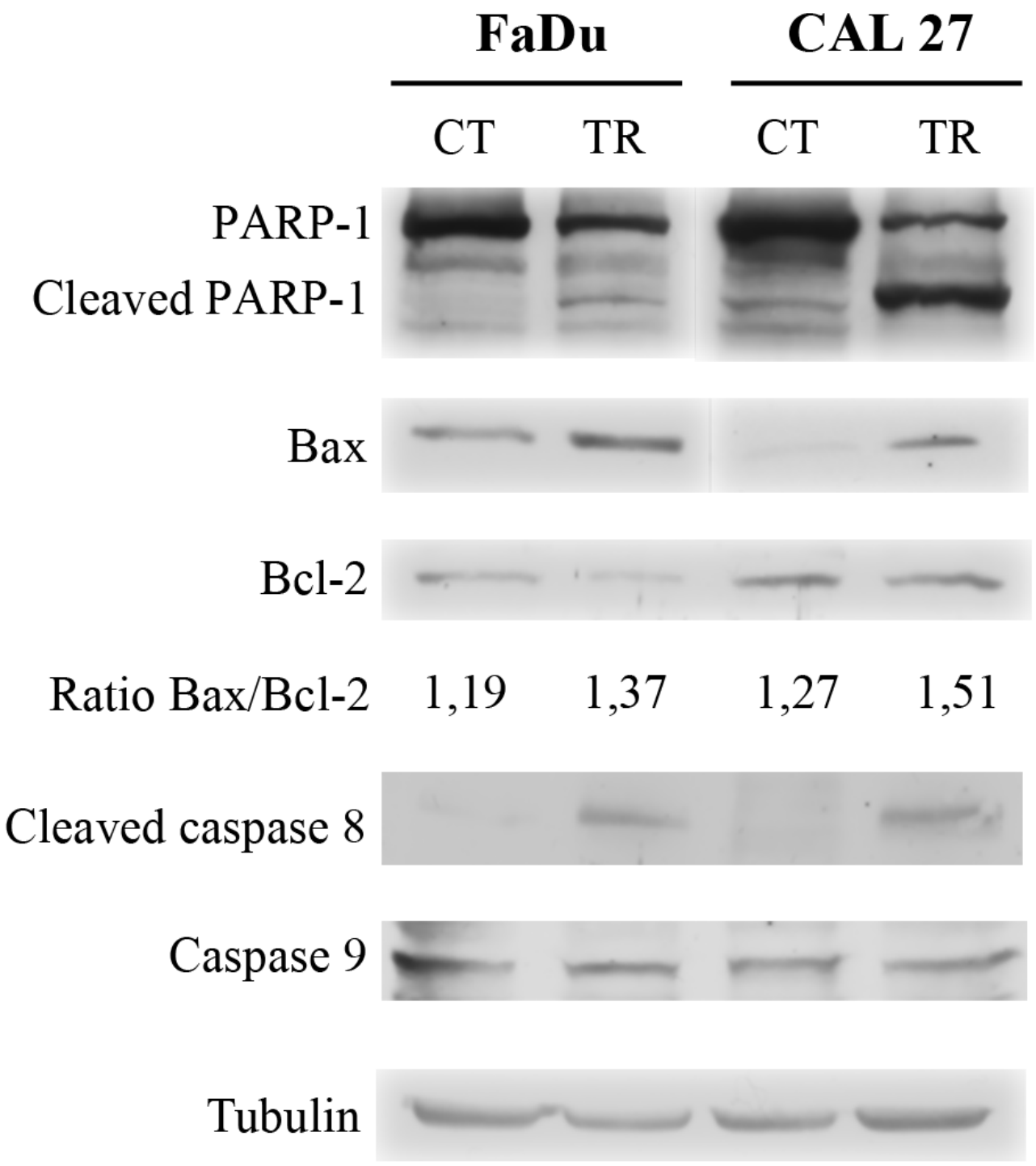

Figure 4

Western blot of PARP-1, Bax, Bcl-2, cleaved caspase 8, caspase 9 and tubulin from FaDu and CAL27 cells untreated (CT) and treated (TR) with 2 μM RDS 60 for 24 h. The means from densitometry quantifications of three different experiments of the Bax to Bcl-2 ratio normalized to tubulin are indicated.

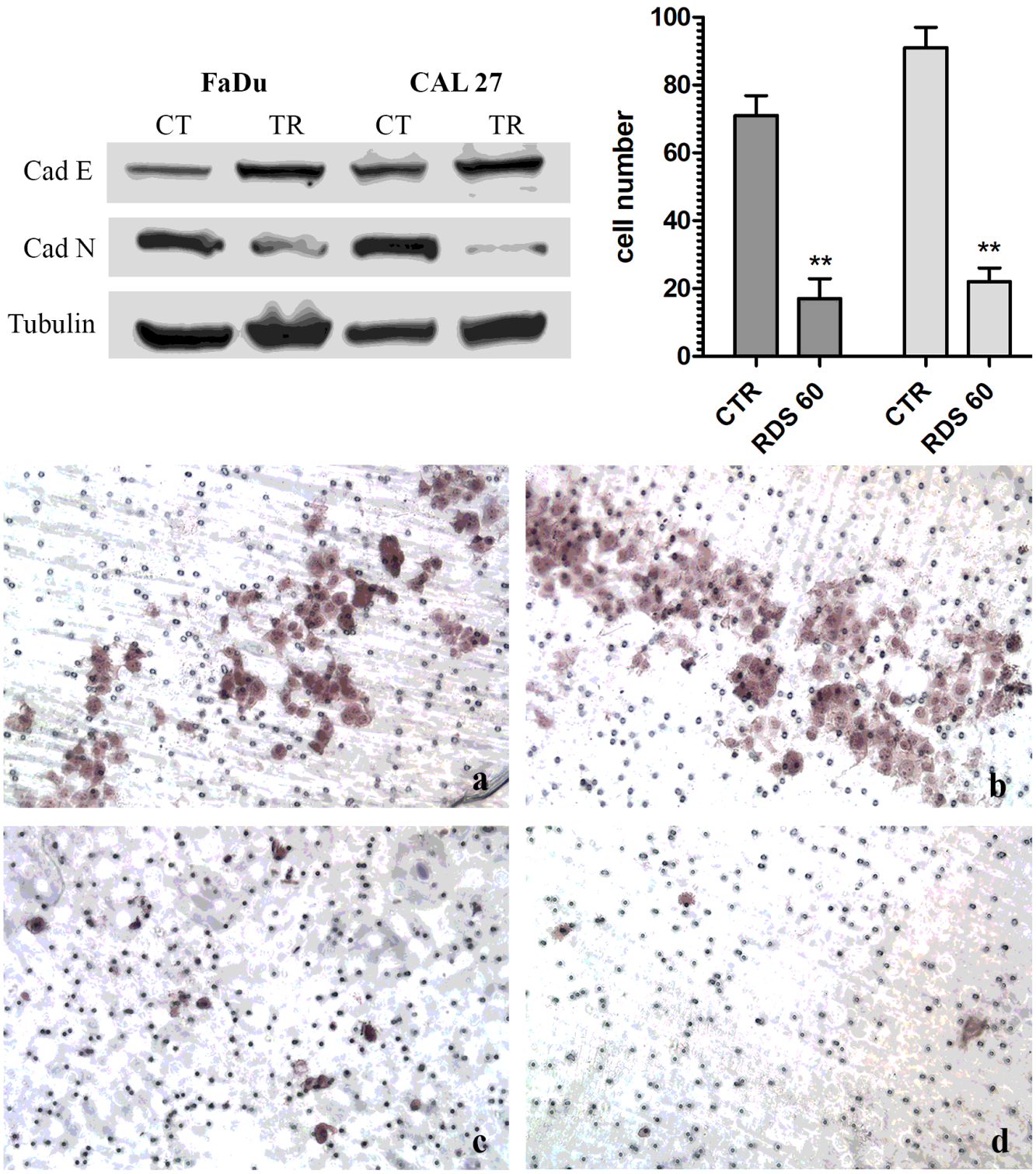

Figure 5

Left upper panel - Western blot of EMT related proteins E-cadherin and N-cadherin for untreated (CT) and 1 μM RDS 60 treated (TR) for 24 h FaDu and CAL27. Lower panel - Matrigel invasion assay of FaDu (a, c) and CAL27 (b, d) cells untreated (a, b) and treated with 1 μM RDS 60 for 16 h (c, d). Right upper panel - Migrated cells in five random fields from three independent experiments were counted and the means±SD are reported in the graphic with **P<0.001.